https://doi.org/10.1016/j.apmt.2019.100546

Spatiotemporal dual-delivery of therapeutic gas and growth factor for prevention of vascular stent thrombosis and restenosis

Qiufen Tu[a,1], Xin Zhao[b,1], Shuai Liu[a], Xiangyang Li[a], Qiang Zhang[b], Han Yu[a], Kaiqin Xiong[a], Nan Huang[a], Zhilu Yang[a,*]

[a] Key Lab of Advanced Technology for Materials of Education Ministry, School of Materials Science and Engineering, Southwest Jiaotong University, Chengdu 610031, China

[b] Department of Biomedical Engineering, The Hong Kong Polytechnic University, Hung Hom, Kowloon, Hong Kong, China

* Corresponding authors. *E-mail addresses*: zhiluyang1029@swjtu.edu.cn (Z. Yang)

[1]Q. Tu and X. Zhao contributed equally to this work.

Abstract:

Injury of endothelium is an inevitable consequence of cardiovascular stent implantation, which increases the incidence of in-stent restenosis (ISR) and late stent thrombosis (LST). Rapid and complete re-endothelialization, along with long-term suppression of smooth muscle cells (SMCs) are mandatory to alleviate these complications. To this goal, we designed a multi-functional stent coating, consisting of a vascular endothelial growth factor/Cu^{II}-dopamine(VEGF/Cu^{II}-DA) complex network for a spatiotemporal delivery of VEGF and nitric oxide (NO). We fabricated such network using a two-step stent-coating process: first a Cu^{II}-DA network with NO catalytic activity via metal-catecholamine coordination chemistry, followed by conjugation of VEGF onto the Cu^{II}-DA network via imine formation. The conjugated VEGF significantly accelerated the early-stage endothelial cell (EC) migration/growth for the first 7 days, forming a new and complete endothelial layer on the lumen. Furthermore, Cu ions sustainably decomposed endogenous S-nitrosothiols (RSNOs) in the bloodstream into NO for over 30 days, suppressing SMC migration/proliferation and ultimately preventing ISR and LST. Altogether, such designed stent coating provides options for a phase-adjusted endothelial repair during cardiovascular treatment.

Keywords:

Cardiovascular stents; Biomimetic multi-functional coating; Spatiotemporal dual-delivery; Vascular endothelial growth factor; Nitric oxide

1. Introduction

Cardiovascular diseases (CVDs) such as coronary artery diseases and stroke are a class of diseases mainly involving the heart and blood vessels [1]. As the leading cause of premature death and chronic disability worldwide - costing over $350 billion - they kill more than 18 million people every year [2]. To treat CVDs, intervention with cardiovascular stents is the most widely performed interventional treatment nowadays, accepting inevitable mechanical injuries of the endothelium [3]. Clinically used cardiovascular stents can be classified into bare metal stents (BMSs) and drug-eluting stents (DESs). Compared with BMSs with no surface modifications or coatings, DESs have polymer coatings loaded with drugs (e.g., sirolimus or paclitaxel) that suppress smooth muscle cell (SMC) migration/proliferation, and can dramatically reduce the restenosis rate from approximately 20% to 5-10% [4,5]. However, the loaded anti-proliferative drugs indiscriminately suppress endothelial cell (EC) growth, leading to a delayed re-endothelialization process with impaired endothelial functions [6,7]. It has to be highlighted that long-term safety concerns of both BMSs and DESs remain because interventional cardiovascular stents inevitably injure the endothelium and trigger a series of cellular responses.

The vascular endothelium plays a central role in maintaining antithrombotic and anticoagulant functions. Disruption of the endothelial layer caused by stent implantation initiates a cascade of cellular events which can be roughly divided into three phases: In phase 1, activated platelets and circulating leukocytes rapidly adhere and aggregate at the implantation site, resulting in acute/subacute inflammation, thrombosis, and subsequent neointimal proliferation [8-10]. In phase 2, ECs migrate to and proliferate at the implantation site for re-endothelialization [11]. If this process is delayed or incomplete, local inflammatory responses due to the platelet/leukocyte aggregation/activation may be extended, with the potential risk of in-stent restenosis (ISR) and late stent thrombosis (LST) [6]. It is, therefore, imperative to promote EC migration and proliferation onto the stent lumen immediately (7-10 days) after stent deployment as the rapidly formed endothelium can serve as a barrier against platelet/leukocyte adhesion [11-13]. At phase 3, SMCs proliferate at the intimal region with extracellular matrix (ECM) deposition for complete wound repair [14,15]. Long-term excessive migration and proliferation of SMCs (up to 1 year) may lead to

maladaptive neointimal proliferation and reduced vessel lumen, leading to late-stage ISR [15,16]. An ideal cardiovascular stent, therefore, should enable early re-endothelialization to prevent platelet/leukocyte aggregation, and subsequently provide long-term inhibition of SMC migration/proliferation to reduce the cascades of cellular responses to prevent ISR and LST.

Considerable efforts have been made over the past decade in modification of the stent surface to improve the safety and efficacy of cardiovascular stents. In addition to maintaining adequate mechanical properties during vascular regeneration to avoid constrictive remodeling, surface modification can further improve hemocompatibility and bioactivity using a variety of biomolecules. Potential candidates for stent surface coating include cell-adhesive peptides (e.g., Arg-Glu-Asp-Val) [17,18] and polydopamine (PDA) to facilitate EC adhesion, proliferation, and migration [19], and nitric oxide (NO)-releasing/generating moieties [20-28]. NO production from the stent compensates for the lack of endogenous NO due to the endothelial damage and retains long-term vascular homeostasis by encouraging EC migration and proliferation while suppressing SMC migration and proliferation [24-28]. Moreover, as a potent vasodilator, the sustained and stable generation of NO can also counter ISR [24,26,28]. However, these NO-releasing/generating coatings are still insufficient to promote rapid and complete re-endothelialization at an early stage; such delayed endothelialization possibly causes in-stent neo-atherosclerosis and very late stent thrombosis (>1 year post-implantation), thus hampering the clinical success of long-term stent implantation [29]. In addition, it is not feasible to enhance vascular endothelium formation by further increasing the amount of NO because excessive NO may damage ECs by altering protein structure and functions, and by the formation of peroxynitrite ($ONOO^-$), a highly reactive cytotoxic compound [30]. Therefore, considering the sequential responses of the body to the implanted stent, it is necessary to combine multiple programmed therapeutic strategies to achieve phase-adjusted vascular healing (accelerated EC migration and growth for re-endothelialization at the early stage, followed by long-term suppression of SMC migration and proliferation) after intervention.

In this work, we developed a multi-functional cardiovascular stent coating consisting of a vascular endothelial growth factor/Cu^{II}-dopamine (VEGF/Cu^{II}-DA) complex network (Scheme 1). We first created the Cu^{II}-dopamine (Cu^{II}-DA) complex using metal-catecholamine coordination chemistry inspired by mussel surface [31]. Cu^{II} is an angiogenic stimulus by up-regulating the expression and secretion of VEGF [32]. It also has excellent glutathioneperoxidase (GPx)-like property, and catalyzes NO generation through decomposing endogenous NO donors (i.e., RSNOs) in circulating blood over a long period to prevent ISR and LST [28]. The outermost surface of the Cu^{II}-DA coating was covalently functionalized with VEGF by Schiff base/Michael addition reaction with DA. VEGF is supplemented as it promotes EC recruitment, adhesion, migration and proliferation [33,34], and inhibits local inflammatory reactions [35], thus suppressing SMC hyperproliferation and reducing the risk of neointimal hyperplasia and thrombosis. Such VEGF-deposited layer is expected to allow fast delivery of VEGF to regulate vascular cell behaviors, facilitate the rapid and complete re-endothelialization immediately after implantation, and counteract the limitations of only NO-releasing/generating coatings, indicated before. Altogether, this surface modification method allows easy transfer to industrial application, due to its simple procedure, high reproducibility, environmentally friendly nature (no involvement of organic solvents) and high bioconjugation efficiency. We envision that this spatiotemporal dual-delivery of therapeutic biomolecule (VEGF) and gas (NO) from cardiovascular stent coating can target vascular repair mechanisms to achieve fast re-endothelialization and prevent ISR and LST, ultimately leading to a phase-adjusted vascular tissue reconstruction.

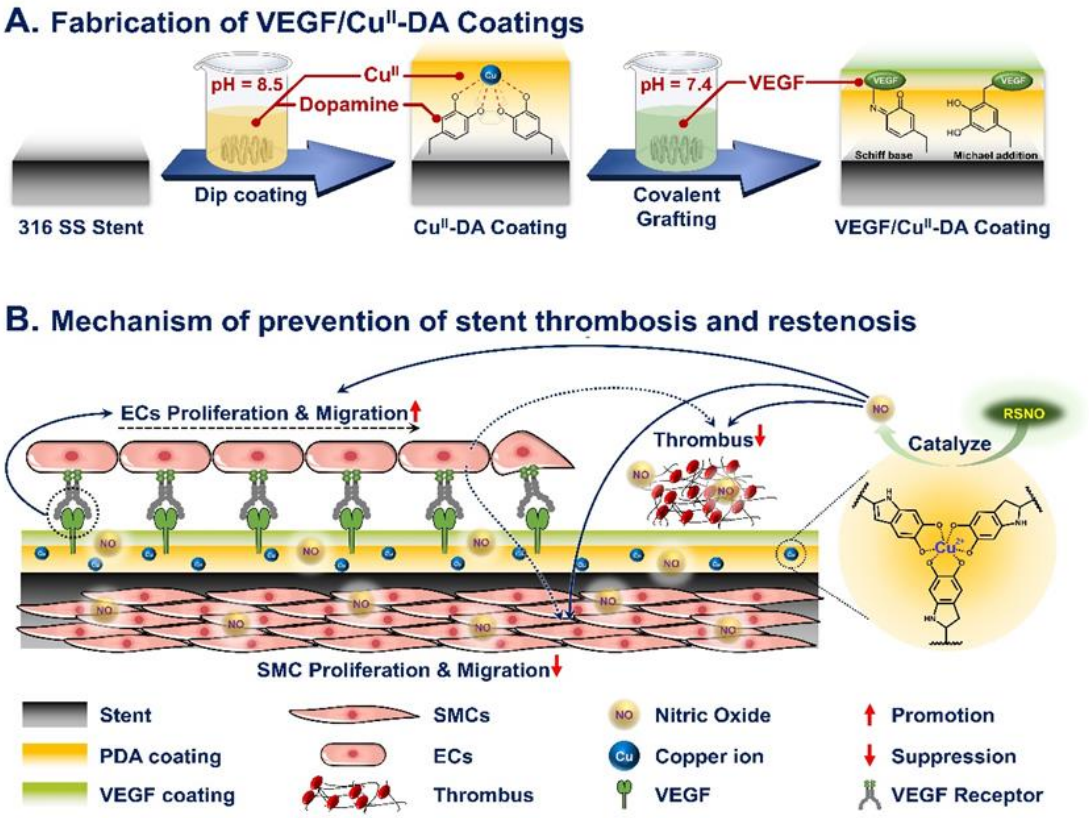

Scheme 1. Schematics showing fabrication and application of the multi-functional VEGF/Cu^{II}-DA coating to spatiotemporally deliver the growth factor VEGF and bioactive nitric oxide (NO) to prevent ISR and LST. (A) Fabrication of the VEGF/Cu^{II}-DA complex coating onto a 316L stainless steel (SS) stents using a simple two-step dip coating approach. The stent was first immersed into an aqueous solution containing copper ions and DA to fabricate the Cu^{II}-DA complex on the stent surface via metal-catecholamine coordination chemistry. Then, the Cu^{II}-DA coated stent was dipped into VEGF solution to covalently immobilize VEGF on the outermost surface of the coating via spontaneous Schiff base/Michael addition reaction. (B) Mechanism of prevention of stent thrombosis and restenosis using the VEGF/Cu^{II}-DA coated stents. The incorporated Cu ions in PDA coating could inhibit inflammation and sustainably decompose the endogenous RSNOs from local fresh blood into NO gas for a long extended period, thus reducing platelet aggregation and activation. The conjugated VEGF in the coating could significantly accelerate the early-stage EC migration and growth, forming a new and complete endothelium on the stent. Furthermore, NO released from RSNOs and the migrated ECs together could suppress the SMC migration/proliferation and reducing the thrombus formation. The spatiotemporal dual-delivery of VEGF and NO enables the fast re-endothelialization of cardiovascular stents followed by long-term prevention of ISR and LST, thus remarkably improving the *in vivo* efficacy and safety of cardiovascular stents.

2. Result and discussion

2.1 Chemical and physical characterization of the metal-catecholamine coating.

As an essential step required to proceed with further analyses on the coatings' applications, the chemical structures, composition, and growth factor binding effects of the Cu^{II}-DA coating were firstly determined. An electron paramagnetic resonance (EPR) spectrum (Bruker A320) was taken to investigate the existing structures of the control, PDA, and Cu^{II}-DA samples (Fig. 1A). While the control and PDA had little presence in their respective samples, a signal of 3440 mT was found in the final group, indicating the formation of Cu^{II}-DA. Matrix-assisted laser desorption ionization mass spectrometry (MALDI-MS, MALDI micro MX time-of-flight mass spectrometer) analysis was performed of the Cu^{II}-DA to study the polymerization mechanism further. The peaks at 362, 511, 619, and 648 m/z (Fig. 1B) were assigned to some possible copper-containing structures due to their high chemical stability in a tetradentate or pentadentate coordination fashion. This would be a corroborative evidence for the chelation of copper ion with phenolic hydroxyl groups of DA derivatives (Fig. 1C, Fig. S1). Other possible structures are listed in Fig. S2.

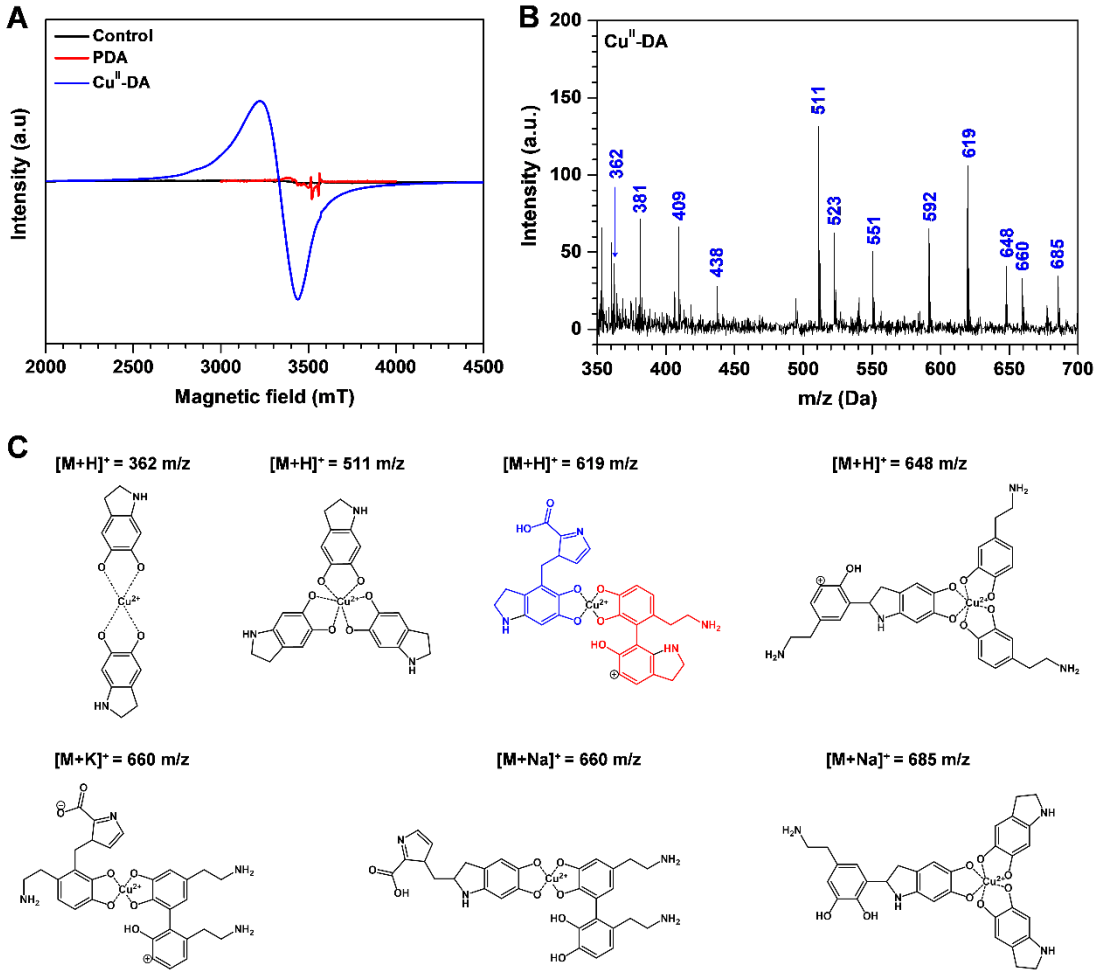

Figure 1. (A) EPR spectra of a control, PDA, and Cu^{II}-DA. (B) MALDI MS spectrum of the Cu^{II}-DA coating. (C) Possible copper-containing structures with high chemical stability in a tetradentate or pentadentate coordination fashion.

The growth factor VEGF can contribute to the biocompatibility and EC proliferation capabilities of surface coatings. It was conjugated to the Cu^{II}-DA coatings for enhanced epithelization [33,34]. Analyses of the chemical structures of PDA, Cu^{II}-DA, and VEGF/Cu^{II}-DA coatings on 316L stainless steel (SS) was performed by grazing incidence attenuated total reflection Fourier transform infrared spectroscopy (GATR-FTIR), as shown in Fig. 2A. SS was used as the surface to host the coatings due to its high biocompatibility, and its predominant application in common stents [36]. Although the basic bond structures of each sample were similar, the peak at 1658 cm^{-1} suggested a C=O bond in the VEGF/Cu^{II}-DA sample, a significant difference expected from the copolymerization of VEGF with Cu^{II}-DA. An X-ray photoelectron spectroscopy (XPS) wide-scan survey spectra analysis was also taken, where the

differences in the chemical compositions of the samples were further verified (Fig. 2B, Table S1). Cu^{II}-DA caused a clear Cu2p signal, copper and nitrogen content were increased, and carbon and oxygen decreased, confirming an alteration in the surface chemical composition of the Cu^{II}-DA-coated samples. Furthermore, the immobilization of VEGF onto the Cu^{II}-DA coating was apparent in a reduced content of copper, carbon, and nitrogen content and increased oxygen content. Quartz crystal microbalance with dissipation monitoring (QCM-D) analysis was adopted to quantify the conjugated VEGF in real-time, and finally about 451 ± 18 ng/cm^2 (n=4) VEGF was conjugated on the Cu^{II}-DA-coated samples, verifying the successful conjugation of VEGF to the Cu^{II}-DA on the stent surface.

Surface wettability of the VEGF/Cu^{II}-DA-coatings is an important property to be assessed. Water contact angle (WCA) measurements provide information about hydrophobicity or hydrophilicity of the surface, as well as changes in the interaction with liquids [37]. The WCAs of the PDA and Cu^{II}-DA-coated samples were found to be 60º, which is more hydrophilic than the untreated 316L SS surface (85°) (Fig. 2C). The immobilization of VEGF on the Cu^{II}-DA-coated samples led to a subsequent decrease in the WCA of the VEGF/Cu^{II}-DA-coated samples (38º), indicating higher hydrophilicity properties. Shin et al. [33] have reported similar findings, in which VEGF/PDA-coated samples had a lower WCA of 52.4 ± 2.4° than the bare poly(L-lactide-co-ε-caprolactone) film attributable to the hydrophilic properties of VEGF and PDA.

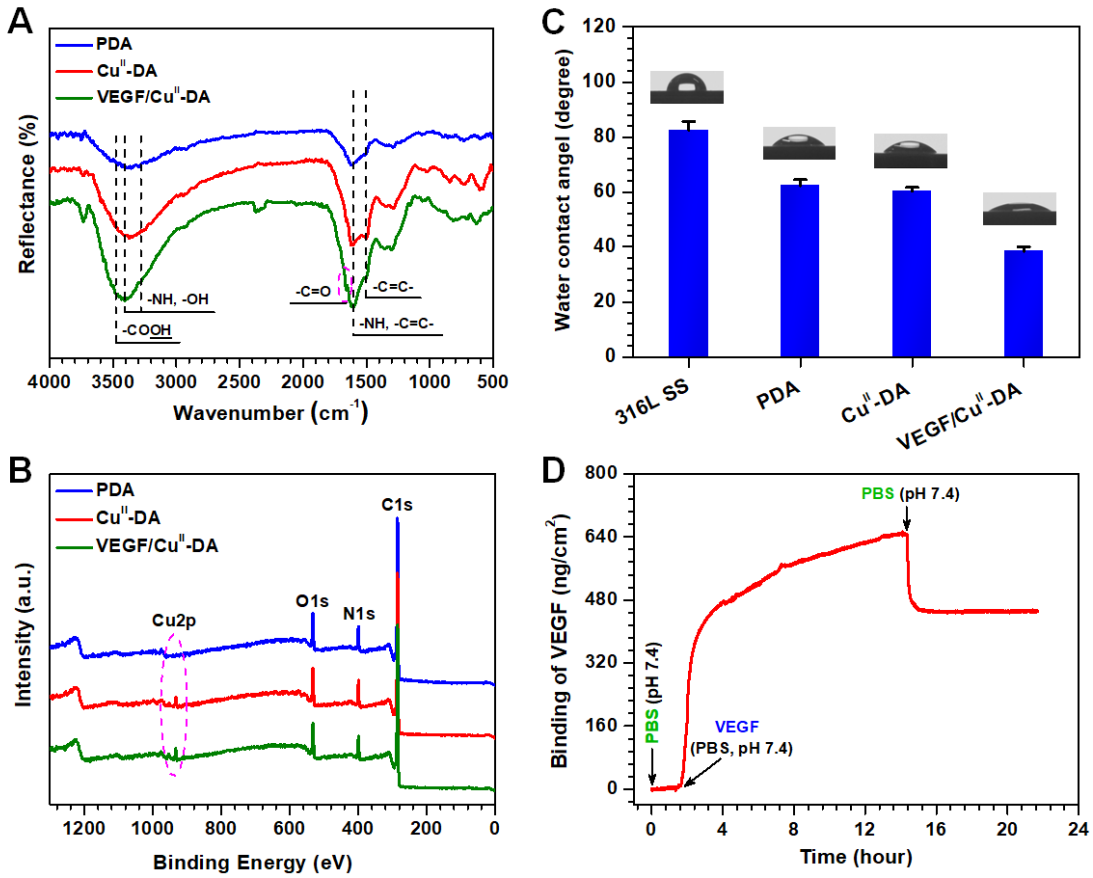

Figure 2. (A) GATR-FTIR spectra of 316L SS, PDA, Cu^{II}-DA, and VEGF/Cu^{II}-DA. (B) XPS wide-scan survey spectra of 316L SS, PDA, Cu^{II}-DA and VEGF/Cu^{II}-DA. (C) Immobilization of VEGF on the Cu^{II}-DA using QCM-D analysis with Q-sense AB. (D) WCAs of 316L SS, PDA, Cu^{II}-DA and VEGF/Cu^{II}-DA. Data presented as mean ± SD (n=4).

2.2 In vitro durability of nitric oxide (NO) generation and mechanical stability.

The EPR and MALDI MS spectrum in Figure 1 confirmed the existence of Cu^{II} in the Cu^{II}-DA and VEGF/Cu^{II}-DA coatings. In the presence of reducing substances such as glutathione (GSH), Cu^{II} was reduced into Cu^{I} and catalyzed NO release from NO donor such as S-Nitrosoglutathione (GSNO) [38]. The release rate and durability of NO from the surface is important for the clinical performance. Cu^{II}-DA and VEGF/Cu^{II}-DA coatings on the 316L SS samples were subjected for 30 days to deoxygenated PBS solution (pH 7.4) with NO donors. The NO release rates were determined in a real-time chemiluminescent assay (Fig. 3A and B). Both the Cu^{II}-DA and VEGF/Cu^{II}-DA coatings did initiate significant NO production 10 min after exposure to the NO donor, and stable catalytic release rates of (5.78 ± 0.49) ×10^{-10} mol×cm^{-2}×min^{-1} (Cu^{II}-DA) and (5.86 ± 0.46) ×10^{-10} mol×cm^{-2}×min^{-1} ($p>0.05$) (VEGF/Cu^{II}-DA) were obtained at 50

minutes, confirming that VEGF immobilization did not affect NO generation of the coating (Fig. 3A). NO production from the NO donor-exposed VEGF/Cu^{II}-DA stent samples continued for 30 days, sustaining 64% of the NO release rate measured immediately after the exposure to the NO donor solution (Fig. 3C). Thus, the VEGF/Cu^{II}-DA-coated samples continuously produced NO beyond 30 days, which is longer than the conventional NO generating Ti-Cu coatings [39]. Such long-term NO generation appears beneficial as it indicates increased chances for successful re-endothelialization and inhibition of stent restenosis and thrombosis.

A VEGF/Cu^{II}-DA-coated 316L SS stent was mounted onto a dilated angioplasty balloon for a stent dilation analysis, as shown in Fig. 3D. The balloon dilation measured a 65 ± 4% increase in diameter, where scanning electron microscopy (SEM) images revealed a dense and homogenous stent coating without cracks and delamination, demonstrating the adaptability of the coating to surface manipulation (Fig. 3D). This adhesion is crucial for *in vivo* application, where a similar set-up is necessary during implantation to adjust to the target accordingly [28]. The mechanical stability and flexibility of the coating, and the efficiency and long-term stability in NO generation confirm the potential of the VEGF/Cu^{II}-DA coatings for therapeutic purposes.

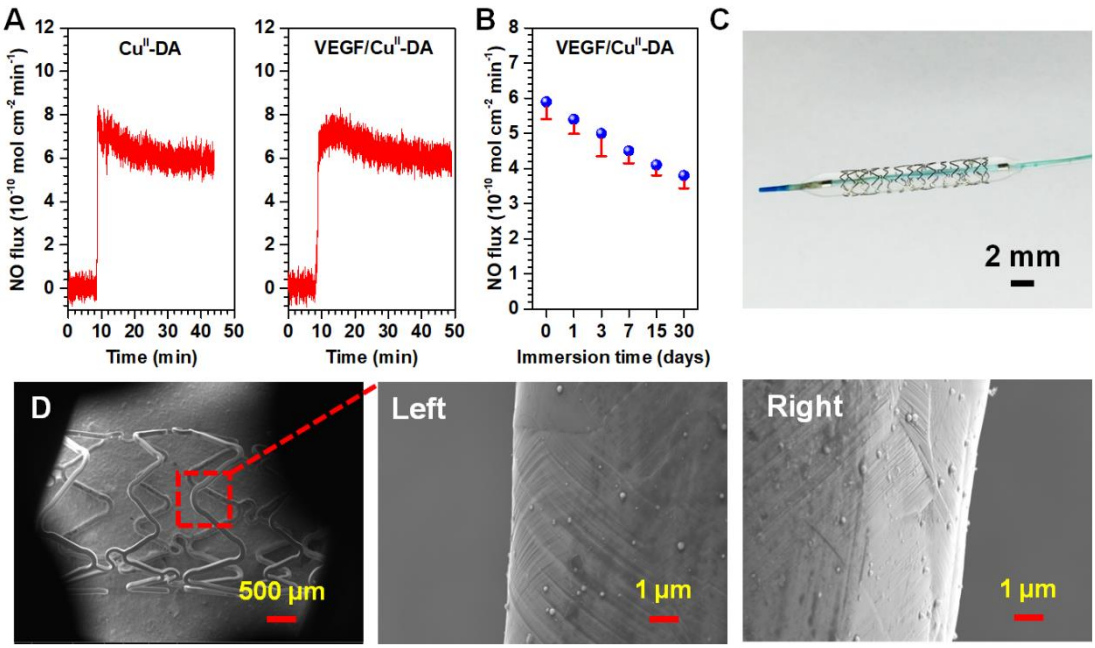

Figure 3. (A) Catalytic NO generation patterns of the Cu^{II}-DA (left) and VEGF/Cu^{II}-DA (right) coating, as well as (B) NO release rates from the VEGF/Cu^{II}-DA after continuous subjection to PBS (pH 7.4) containing NO donors. The NO donor solutions were replaced every 12 h, and

the release rates were monitored using the NO analyzer Seivers 280i. (C) Image taken with a digital camera of a dilated angioplasty balloon carrying a 316L SS stent sample coated with a VEGF/Cu^{II}-DA coating and (D) SEM micrographs taken with Quanta 200 of dilated VEGF/Cu^{II}-DA-coated 316L SS.

2.3 In vitro biological properties of metal-catecholamine coatings.

The promotion of appropriate cell adhesion and proliferation is desired on an ideal biocompatible surface coating. The production of a physiological NO concentration induced by exposure to the NO-donating solution can enhance EC growth for improved cell repair [20]. Thus, *in vitro* studies were performed using human umbilical vein endothelial cells (HUVECs) with and without the presence of NO-donor supplements to examine their behaviors. Cell morphology of the HUVECs cultured on 316L SS, PDA, Cu^{II}-DA, and VEGF/Cu^{II}-DA surfaces for 2, 24, and 72 h showed little difference between the samples, regardless of the presence of NO-donating supplements (Fig. 4A, Fig. S3). Adhesion of the HUVECs, however, was significantly enhanced 2h after seeding onto the VEGF/Cu^{II}-DA coating, particularly in comparison to the 316L SS coatings. This difference was further enhanced with NO donors. The VEGF/Cu^{II}-DA sample showed a HUVEC cell density of 539 ± 39.9 cell/cm^2 adherent to the surface after 2 h of culture, while the 316L SS sample only had 315 ± 44.1 cells/cm^2 (Fig. 4B). HUVEC proliferation was also examined in Fig. 4C. The VEGF/Cu^{II}-DA surface resulted in the highest cell viability after 72 h, in comparison to 316L SS. Fluorescent imaging further revealed an enhanced HUVEC migration on the VEGF/Cu^{II}-DA coating under NO-promoting conditions (Fig. S6). This enhanced HUVEC adhesion and proliferation exceeded values for Cu^{I} and Cu^{II} coatings without growth factor reported by Luo et al. [40], or the REDV- amphiphile/Dopa-amphiphile coatings studied by Ceylan et al [41]. Because HUVEC adhesion and proliferation showed significant difference in the presence versus absence of NO-donating supplements, it is concluded that the NO generation provided the strongest promotion of HUVEC adhesion and proliferation.

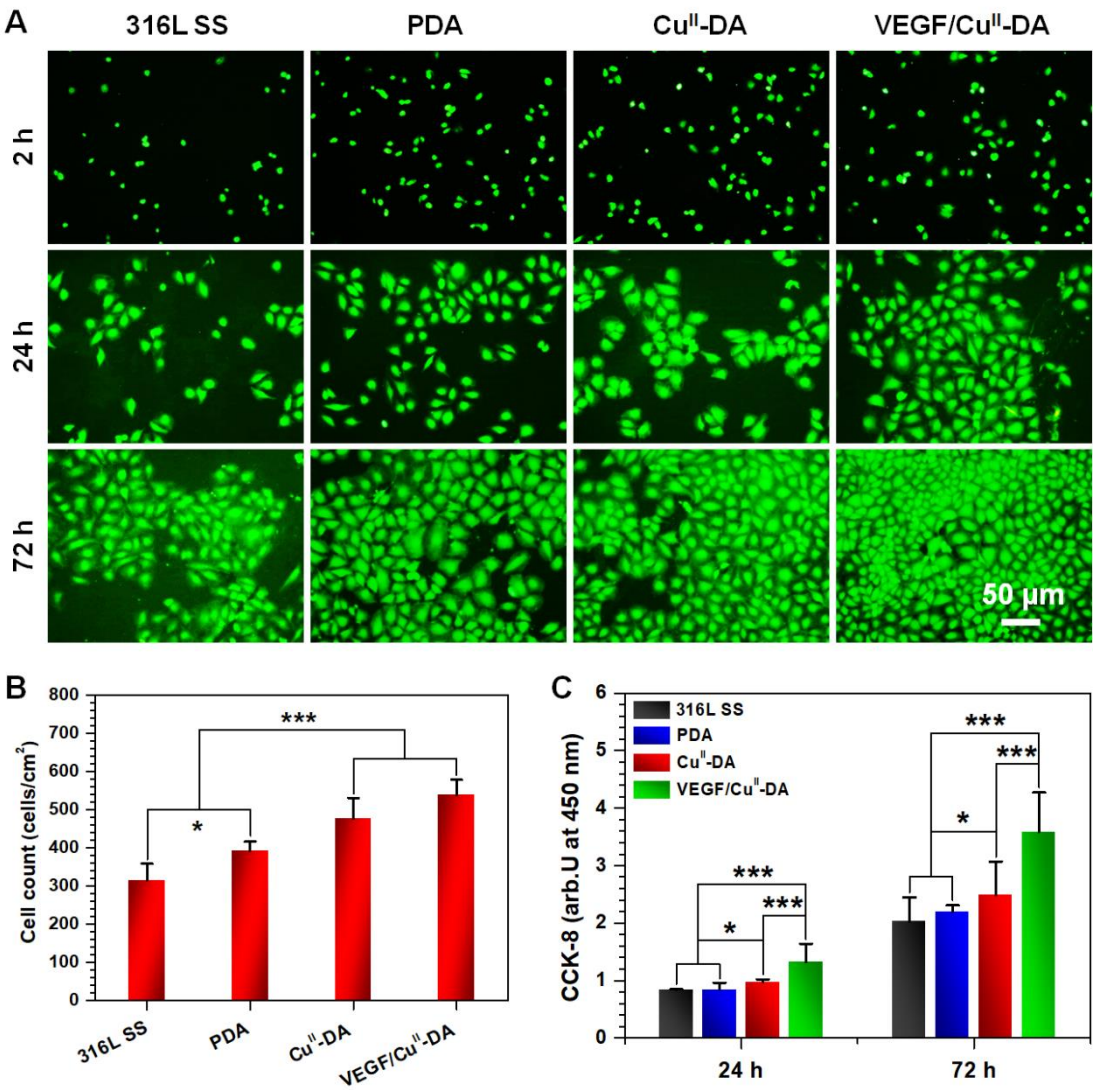

Figure 4. Adhesion and proliferation of HUVECs cultured in media containing NO donor (10 μM GSNO and 10 μM GSH). (A) Fluorescent staining of HUVECs cultured on bare 316L SS, PDA, Cu^{II}-DA and VEGF/Cu^{II}-DA samples for 2, 24 and 72 h. (B) Quantification of HUVECs onto the samples after 2 h of incubation (n=12). (C) Proliferation of HUVECs grown on the samples after 24 and 72 h of incubation. Data presented as mean ± SD (n = 4) and analyzed with a one-way ANOVA (*$p < 0.05$, ***$p < 0.001$).

Additionally, inappropriate overproliferation and migration of cells may also be harmful, such as overgrowth and migration of SMCs, as it frequently occurs after stent implantation in ISR [10,16]. The inhibitory effect of the VEGF/Cu^{II}-DA coating on adhesion and proliferation of human umbilical artery smooth muscle cells (HUASMCs) was tested in the presence and absence of NO donors. In a similar fashion to the HUVEC studies, the HUASMCs were cultured on the four sample coatings in presence

or absence of NO donor and observed after 2, 24, and 72 h. The VEGF/Cu^{II}-DA coating in the presence of NO donors showed significant suppression of HUASMCs compared to the bare 316L SS (Fig. 5A, Fig. S4). Numerical evaluation of the cell adhesion after 2 h (Fig. 5B) confirmed this impression. The NO donor-absent samples did not inhibit HUASMC adhesion. VEGF/Cu^{II}-DA also inhibited the viability of HUASMCs, determined by the metabolic CCK-8 (Cell Counting Kit-8) assay (Fig. 5C). Metabolic activity of HUASMCs on VEGF/Cu^{II}-DA increased only slightly from 24 h to 72 h culture (1.05 ± 0.09 OD to 1.90 ± 0.10 OD, respectively), in comparison to a prominent change on bare 316L SS (1.25 ± 0.01 OD to 3.10 ± 0.14 OD, respectively). Observations on cell migration using fluorescence images revealed negligible cell migration on the VEGF/Cu^{II}-DA coatings in the presence of NO donor supplements (Fig. S7). The Cu^{I} and Cu^{II} coatings without VEGF, developed by Luo et al. [39] displayed only weak inhibition of HUASMC attachment. The VEGF component of the VEGF/Cu^{II}-DA coatings, therefore, apparently improved the ability to inhibit attachment and proliferation of HUASMCs from the NO generation.

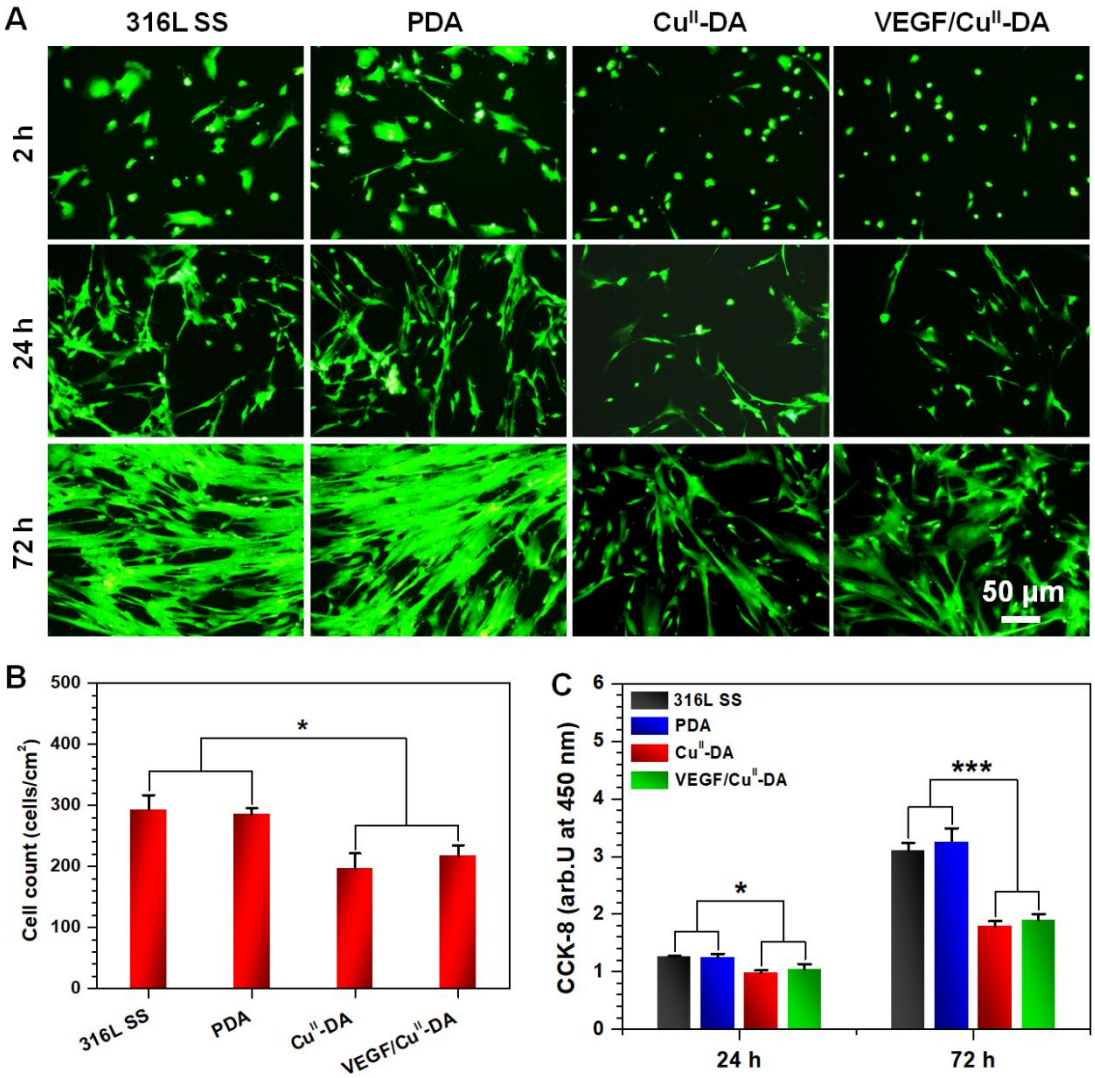

Figure 5. Adhesion and proliferation of HUASMCs cultured in media containing NO donor (10 μM GSNO and 10 μM GSH). (A) Fluorescent staining of HUASMCs on 316L SS, PDA, Cu^{II}-DA and VEGF/Cu^{II}-DA samples after culture for 2, 24 and 72 h. (B) Quantification of HUASMCs onto samples after 2 h of incubation (n = 12). (C) Proliferation of HUASMCs grown on the samples after 24 and 72 h of incubation. Data presented as mean ± SD (n = 4) and analyzed with a one-way ANOVA (*$p < 0.05$, ***$p < 0.001$).

Previously, we have found that re-endothelialization is influenced by the competition of EC and SMC [26-28]. To understand the effect of our coating on EC and SMC behaviours, HUVECs and HUASMCs were co-cultured on the four surfaces and examined 2 and 24 h after seeding. As illustrated in Fig. 6A, a significant increase in HUVECs (green) and decrease in HUASMCs (red) was evident, which was enhanced particularly on the VEGF/Cu^{II}-DA coating with NO donor supplements. In contrast,

samples co-cultured in the absence of NO donor supplements exhibited negligible differences between the numbers of the two cell types (Fig. S5). The ratios of the two cell types were calculated and compared for the different time points (Fig. 6B and C). Obviously, the increase in the levels of HUVECs and the subsequent decrease in levels of HUASMCs are most visible on the NO donor-exposed VEGF/Cu^{II}-DA coating, indicating the promotion of HUVEC adhesion and proliferation with the simultaneous repression of HUASMC adhesion and proliferation. The NO-generating VEGF/Cu^{II}-DA coatings have the ability to inhibit or enhance adhesion and proliferation of SMC and EC, respectively, providing a biocompatible microenvironment for vessel wall healing.

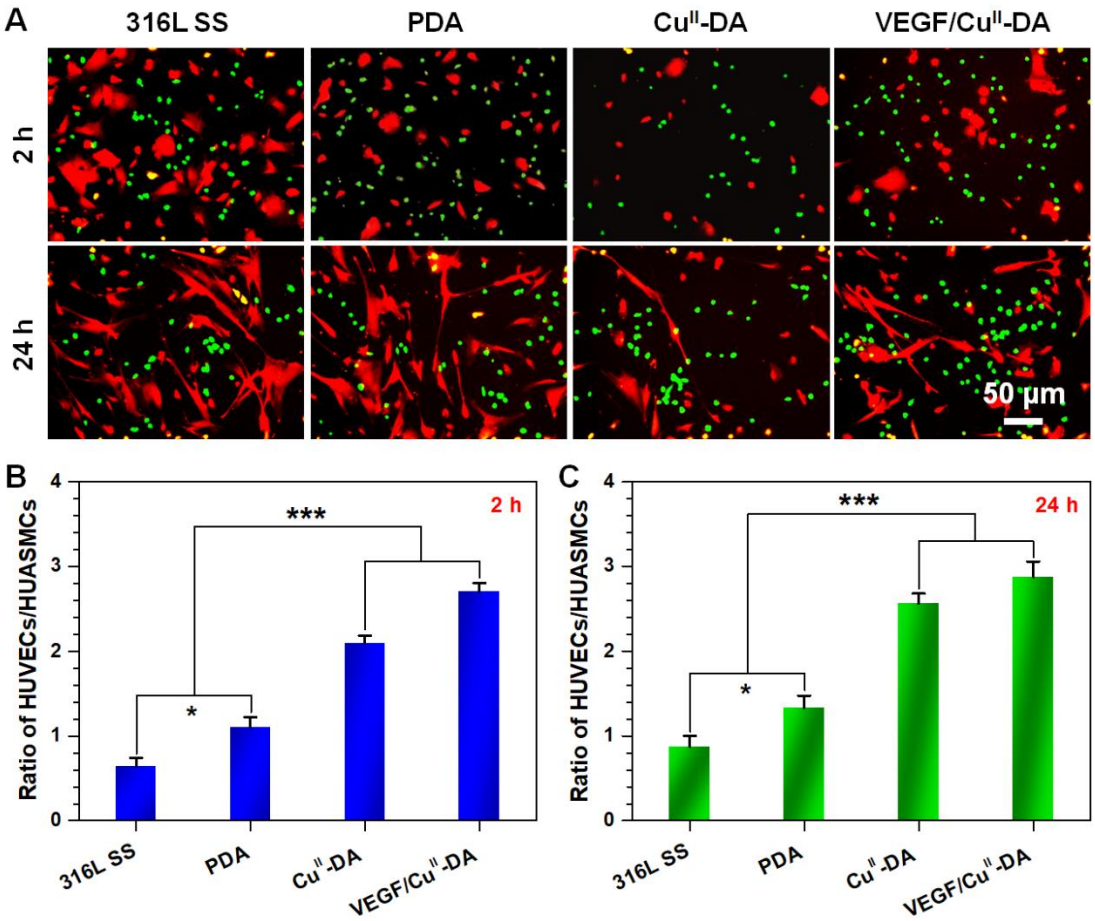

Figure 6. HUVECs and HUASMCs co-cultured in cell culture media supplemented with NO donor (10 μM GSNO and 10 μM GSH). (A) Cell tracker green CMFDA staining of HUVECs (green) and red CMTMR staining of HUASMCs (red) after 2 and 24 h co-culture on the 316L SS, PDA, Cu^{II}-DA, and VEGF/Cu^{II}-DA samples. The ratio of HUVECs *vs.* HUASMCs grown on different sample surfaces was calculated for (B) 2 and (C) 24 h. Data presented as mean ± SD (n = 16) and analyzed using a one-way ANOVA (*$p < 0.05$, ***$p < 0.001$).

2.4 Ex vivo thrombogenic potential of coated stents.

The VEGF/Cu^{II}-DA coating was subjected to an *ex vivo* blood circulation study to analyze its anti-thrombogenicity. Arteriovenous shunts of polyvinyl chloride (PVC) tube from the carotid artery to the jugular vein were prepared in New Zealand white rabbits for the thrombogenic assay. Uncoated and VEGF/Cu^{II}-DA-coated 316L SS foils were installed into two parallel shunt tubes (Fig. 7A). The samples were subjected to blood flowing through the arteriovenous shunts for 2 h, where the VEGF/Cu^{II}-DA-functionalized 316L SS foils displayed a significantly lower clot thrombus formation than the bare SS foil (Fig. 7B). The occlusion rates of the circuits with the VEGF/Cu^{II}-DA-coated 316L SS foils were significantly reduced compared to the uncoated 316L SS foils (11.8 ± 2.3% *versus* 86.4 ± 4.7%, respectively, Fig. 7C). The occlusion rate also reflects in the blood flow rates during circulation. We also found that the VEGF/Cu^{II}-DA-coated circuit retained a significantly higher blood flow rate of 90.1 ± 9.1% of the initial flow rate, greatly exceeding that of the uncoated circuits at 18.7 ± 7.4% (Fig. 6A).

The reduced clot formation on the VEGF/Cu^{II}-DA-coated foils was also visible in the thrombus weight (Fig. 7D and E). The weight of the thrombus on the VEGF/Cu^{II}-DA sample was 1.7 ± 1.2 mg, compared to 19.2 ± 4.2 mg on the uncoated samples ($p<0.001$). Scanning electron microscopy (SEM) images of the sample surfaces after *ex vivo* circulation, indicate apparent thrombus formation on the uncoated samples with a fibrin network entrapping a large number of red blood cells, whereas on the VEGF/Cu^{II}-DA-coated samples there was only a small amount of platelets adherent with a low degree of activation (Fig. 7F). These results from the *ex vivo* circulation demonstrate that the NO-inducing VEGF/Cu^{II}-DA-coated 316L SS foils provided enhanced anti-thrombogenic properties.

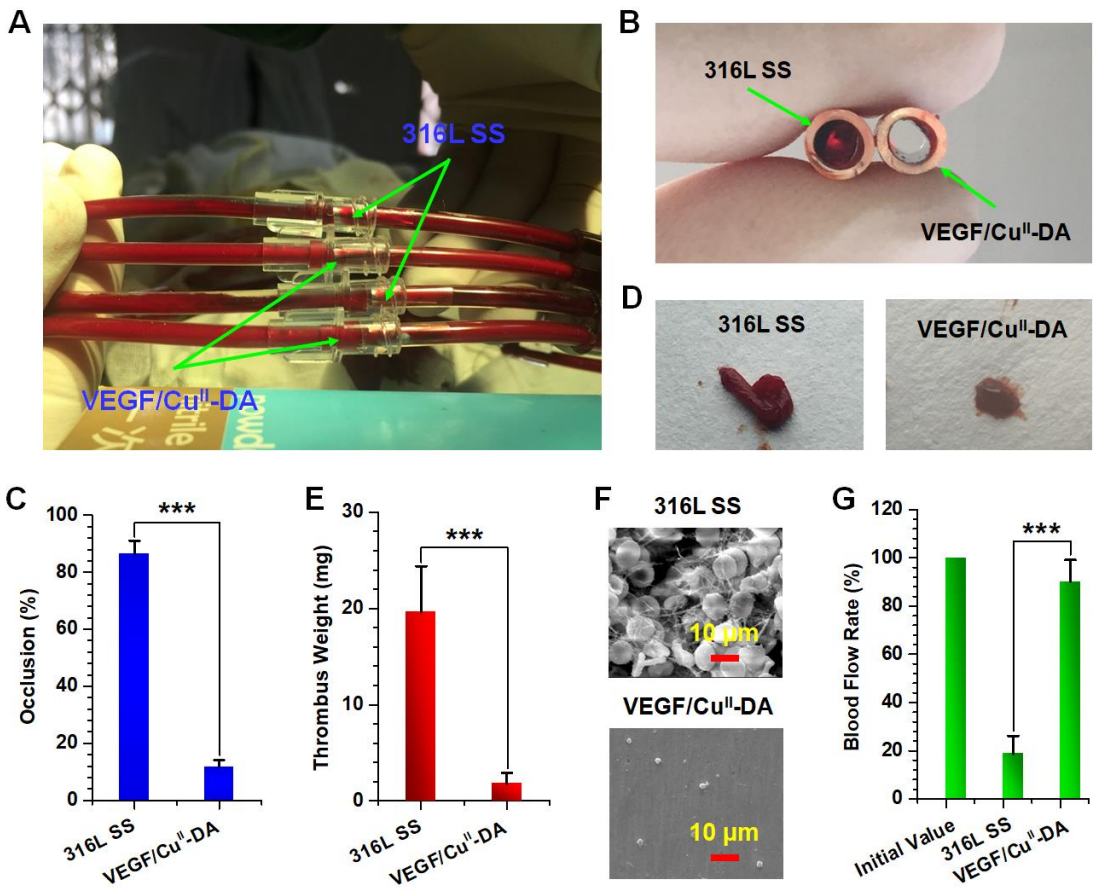

Figure 7. Thrombogenicity of the VEGF/Cu^{II}-DA-coated 316L SS foils in a New Zealand white rabbit arteriovenous shunt model; NO donor (10 μM GSNO and 10 μM GSH) was additionally supplemented in blood during the circulation. (A) Image of the *ex vivo* circulation thrombogenicity assay of a rabbit. (B) Images of cross-sectioned tubing containing uncoated and VEGF/Cu^{II}-DA-coated 316L SS foils exposed for 1.5 h to blood flow in a rapid arteriovenous shunt model (C) Percent occlusion of the circuits'cross-sectional area. (D) Photographs of the thrombi formed on the uncoated and VEGF/Cu^{II}-DA-coated 316L SS foils. (E) Thrombus weight on the uncoated and VEGF/Cu^{II}-DA-coated 316L SS samples. (F) SEM images of platelet adhesion on the uncoated and VEGF/Cu^{II}-DA-coated 316L SS surface. (G) Blood flow rates of the uncoated and VEGF/Cu^{II}-DA-coated 316L SS generated using different circuits at the end of *ex vivo* circulation. Data presented as mean ± SD (n = 4) and analyzed using a one-way ANOVA (***$p < 0.001$).

2.5 In vivo stent implantation.

An *in vivo* stent implantation was performed in rabbit iliac arteries to examine the effects of VEGF/Cu^{II}-DA coating on restenosis and re-endothelialization. CD31 (Platelet endothelial cell adhesion molecule-1, PECAM-1/CD31) immunofluorescent

stain of the vascular stents implanted *in vivo* for one week was carried out to identify whether the cells on the stent surface were ECs. The results detected via laser confocal microscope showed that VEGF/Cu^{II}-DA-coated stent was covered by a confluent monolayer of cells with strong positive expression of CD31, which was inferred as EC monolayer; however, on the uncoated 316L SS stent, CD31 fluorescence signals can hardly be detected (Fig. 8A), indicating the VEGF/Cu^{II}-DA coating had the ability to accelerate re-endothelialization. Relative fluorescence intenisty of CD31 analyzed by Image J further demonstrated a stronger flurorescence intensity on the surface of the VEGF/Cu^{II}-DA-coated stent than the bare 316L SS stain (Fig. 8D). SEM images of the stents after 1 and 3 months implantation also showed significantly greater re-endothelialization on the VEGF/Cu^{II}-DA coating compared to the naked 316L SS stent surface (Fig. 8B). The VEGF/Cu^{II}-DA-coated stent was covered by a compact monolayer of ECs at 1 month, which formed a thinner layer of intima at 3months, and an overall defined stent profile. In contrast, the uncoated stent observed in one month was not fully covered by an EC layer, followed by obvious intimal hyperplasia making the outline of the stent unclear.

Van Gieson's stains (acid fuchsin& picric acid) of hard tissue sections were used for histomorphometric analysis. The VEGF/Cu^{II}-DA-coated stents showed reduced neointimal hyperplasia, visible in the wider artery lumens, compared to narrow lumens at the uncoated stents, indicating that the VEGF/Cu^{II}-DA-coated stents suppressed restenosis (Fig. 8C). This was further examined by measuring the mean neointimal area at 1 and 3 months after implantation. We found that the VEGF/Cu^{II}-DA-coated stents maintained a low mean neointimal area with 2.3 ± 0.48 mm^2 at 1 month and 3.6 ± 0.79 mm^2 at 3 months, while the uncoated stents displayed a drastic increase of the mean neointimal area from 4.52 ± 0.68 mm^2 at 1 month to 9.87 ± 0.91 mm^2 at 3 months (Fig. 8E). Neointimal stenosis percentage was also quantified of the stent samples, where the uncoated stents exhibited an extreme increase from $19.8 \pm 4.6\%$ to $37.4 \pm 4.9\%$, whereas the VEGF/Cu^{II}-DA-coated stents increased insignificantly from $9.7 \pm 2.7\%$ to $15.3 \pm 1.9\%$ (Fig. 8F), indicating the capability of the VEGF/Cu^{II}-DA-coating to suppress the ISR.

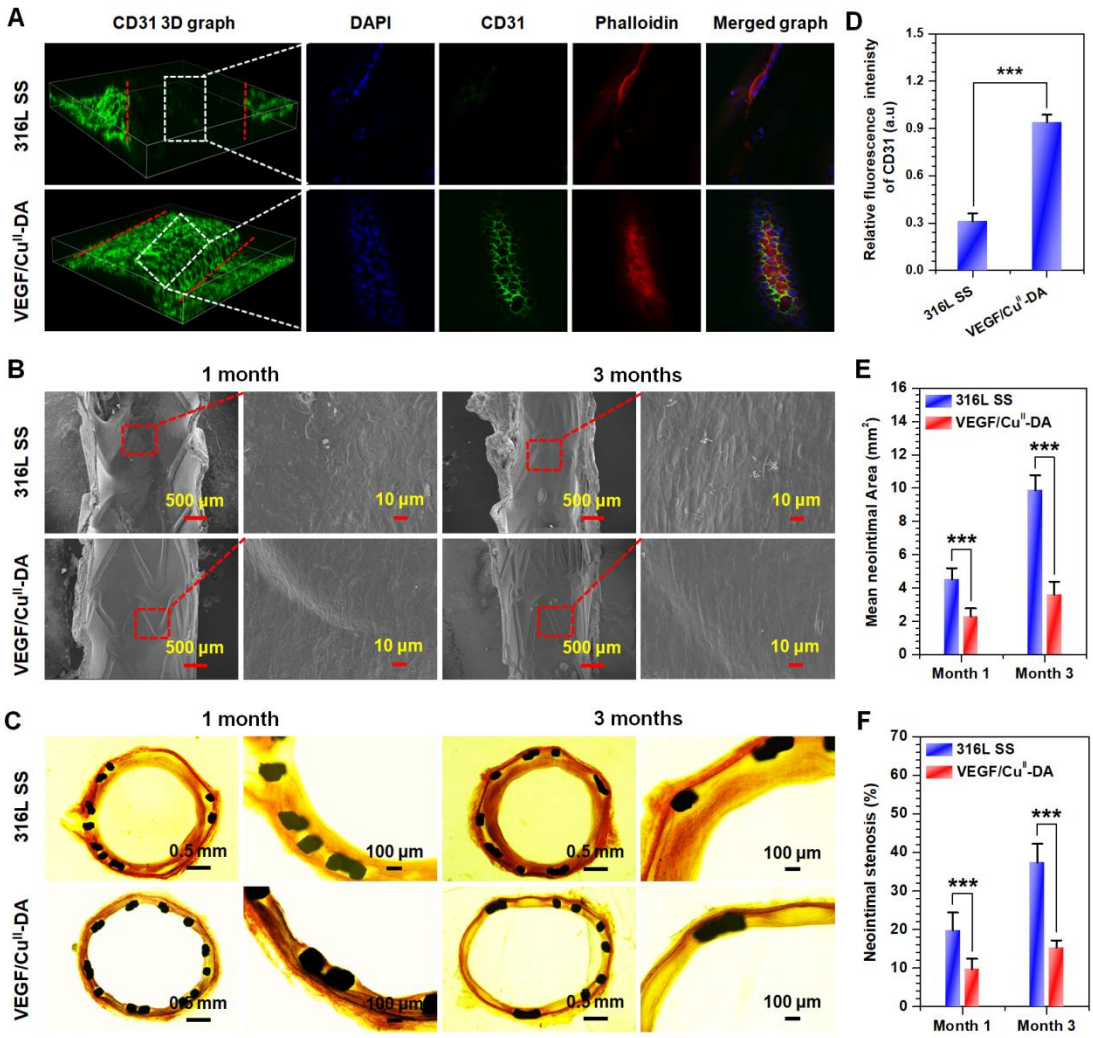

Figure 8. Cardiovascular stents with and without VEGF/Cu^{II}-DA coatings for enhanced re-endothelialization and reduced restenosis. (A) Re-endothelialization of uncoated and VEGF/Cu^{II}-DA-coated 316L SS stents after implantation for 1 week detected by laser confocal microscope after CD31 immunofluorescence, phalloidin and DAPI stain. Stent strut was between two red dotted line, and the white rectangular dashed frame is the uppermost layer of the strut. (B) Re-endothelialization of uncoated and VEGF/Cu^{II}-DA-coated 316L SS stents after implantation for 1 and 3 months observed using SEM. (C) Histomorphometric analysis on ISR at bare 316L SS and VEGF/Cu^{II}-DA-coated stents using Van Gieson's staining of hard tissue slices. (D) Mean fluororescence intensity of CD31 for bare 316L SS and VEGF/Cu^{II}-DA-coated stents in (A). (E) Neointimal area and (F) neointimal stenosis analysis of uncoated and VEGF/Cu^{II}-DA-coated 316L SS stents (n=3). Data presented as mean ± SD and analyzed using a one-way ANOVA (***$p < 0.001$).

3. Conclusion

In summary, we present here a multi-functional VEGF/Cu^{II}-DA stent coating capable of spatiotemporal dual-delivery of the growth factor VEGF and therapeutic gas NO. This coating was conveniently prepared on cardiovascular stents by facile and sequential immersion in metal-catecholamine and VEGF solutions via metal-catecholamine coordination chemistry and spontaneous Schiff base/Michael addition reaction, respectively. The rapid endothelialization and long-term catalytic generation of NO thanks to the grafted VEGF and incorporated Cu ions, respectively, endowed the stents with excellent and long-term anti-coagulation and anti-intimal hyperplasia properties. Altogether, our data suggest that the VEGF/Cu^{II}-DA coating enables the fast re-endothelialization of stents followed by prevention of ISR and LST, providing the potential to be a feasible and effective coatings strategy to improve the clinical efficacy and safety of cardiovascular stents.

4. Experimental section

4.1 Preparation of PDA, Cu^{II}-DA, and VEGF/Cu^{II}-DA coatings.

PDA, Cu^{II}-DA and VEGF/Cu^{II}-DA coatings were prepared on 316L SS discs and vascular stents (Ø 1.65 mm, 18 mm) respectively. In detail, the 316L SS discs and vascular stents were immersed in 0.25 mg/mL dopamine hydrochloride solution with 0 and 5 μg/mL $CuCl_2$ for 24 h at 25 ℃ to construct the PDA and Cu^{II}-DA coatings. Then the samples were cleaned in ion-free water using ultrasound to remove loosely attached molecules and ions. The Cu^{II}-DA samples were sterilized by UV light and then immersed in 0.5 μg/mL sterile VEGF solution in PBS (pH 7.6) for 12 h at 37 °C to prepare the VEGF/Cu^{II}-DA samples.

4.2 Surface characterization.

Electron paramagnetic resonance (EPR) spectra of the PDA, Cu^{II}-DA and VEGF/Cu^{II}-DA coatings were detected to analyze the possible antiferromagnetic coupling of Cu^{2+} ions using a Bruker A320 instrument with appropriate receiver gain, modulation amplitude, modulation frequency, and microwave power. Matrix-assisted laser desorption ionization mass spectrometry (MALDI MS) analyses of the Cu^{II}-DA coatings were obtained by a MALDI micro MX time-of-flight mass spectrometer (Waters, Milford, MA) to reveal the possible reaction manner between the Cu^{2+} ions

and the dopamine molecules. Chemical structures of the PDA, Cu^{II}-DA and VEGF/Cu^{II}-DA coatings were determined by Fourier transform infrared spectroscopy (GATR-FTIR, Nicolet 5700, America) in the range of 4000-400 cm. The surface elemental composition of the coatings mentioned above was analyzed using X-ray photoelectron spectroscopy (XPS, XSAM800, Kratos Ltd, UK) at 12kV×15 mA and a pressure of 2×10^{-7} Pa. The C1s peak (binding energy 284.8 eV) served as a reference for charge correction. WCA was detected using a contact angle meter (DSA100, KrüssGmbH, Hamburg, Germany) and calculated by DSA 1.8 software. QCM-D equipment (Q-sense AB, Sweden) was used to quantify the weight of VEGF covalently immobilized onto the Cu^{II}-DA coating. Quartz crystals (AT-cut, 5 Hz, Ø 10 mm) were coated with Cu^{II}-DA and mounted in the QCM-D equipment chamber, and then VEGF solution (0.5 μg/mL, pH 7.6) was continuously perfused into the chamber until the curve equilibrated. Finally, PBS was perfused to remove the weakly bound VEGF. The mass shift of immobilized VEGF *vs*. time curve was recorded using QTools modeling software.

4.3 Catalytic NO generation.

The Cu^{2+} ions in the Cu^{II}-DA and VEGF/Cu^{II}-DA coatings cancatalyze the NO formation from the donor RSNO in the presence of the reducing agent glutathione (GSH). The generated NO was determined in real-time using a chemiluminescence NO analyzer (NOA 280i, Sievers, Boulder, CO, USA). Briefly, the Cu^{II}-DA and VEGF/Cu^{II}-DA coatings were prepared on 316L SS foils (5 cm × 1 cm). 5 mL of PBS containing 10 μM RSNO and 10 μM GSH was injected into the reactor of NO analyzer, then the Cu^{II}-DA and VEGF/Cu^{II}-DA samples were immersed into the reactor for at least 40 min. The real-time NO release curve was recorded, and the amount of NO was calculated according to calibration curves. To investigate the sustained NO catalytic abilities, the samples were immersed in PBS containing NO donor for 1, 3, 7, 15 and 30 days respectively, where the donor solution was replaced every 12 h. The NO formation of the samples treated with NO donor was detected as above.

4.4 Adhesion, proliferation, and migration of HUVECs and HUASMCs.

As the growth behavior of vascular cells on vascular stents is the significant factor of their long-term function, the influence of Cu^{II}-DA and VEGF/Cu^{II}-DA coatings on

vascular cells should be systematically investigated. For adhesion of a single cell type, HUVECs or HUASMCs at a density of 5×10^4 cells/cm^2 were seeded on 316L SS discs (Ø 1 cm) with PDA, Cu^{II}-DA and VEGF/Cu^{II}-coatings and cultured in complete medium (DMEM/F12 supplemented with 15% FBS for HUASMCs and additionally 15 ng/ml VEGF for HUVECs) with or without NO donor supplement (10 μM SNAP and 10 μM GSH). The NO donor was replenished every 6 h. Samples were taken out after 2 h, 1 and 3 days, fixed with paraformaldehyde and stained by rhodamine for fluorescence detection. Cell proliferation was evaluated by CCK-8 according to the manufacturer's instruction.

For the study of the competitive adhesion of HUVECs and HUASMCs, HUASMCs were labeled with Cell Tracker Orange CMTMR, and HUVECs labeled with Cell Tracker Green CMFDA (Thermo Fisher Scientific Inc, USA). The labeled HUVECs and HUASMCs were respectively resuspended in DMEM/F12 medium with 15% FBS with or without NO donor to a concentration of 5×10^4 cells/mL. Then, 0.5 mL of HUVECs and HUASMCs cell suspension were mixed and seeded onto the samples in a 24-well cell culture plate and cultured under standard cell culture conditions for 2 and 24 h. Then the cells on the samples were observed using a fluorescence microscope (IX51, Olympus, Japan), and the numbers of adherent HUVECs and HUASMCs were counted from at least 12 images.

The migration of HUVECs and HUASMCs on PDA, Cu^{II}-DA, and VEGF/Cu^{II}-DA coatings were investigated as described previously [42]. Briefly, the 316L SS foils (15 cm × 10 cm) were symmetrically folded to form a right angle. The PDA, Cu^{II}-DA, and VEGF/Cu^{II}-DA coatings were deposited onto one of the vertical planes. HUVECs or HUASMCs were seeded on the bare vertical plane at a density of 5×10^5 cells/cm^2 and cultured for 6 h to ensure the formation of a confluent cell layer, then the samples were turned, allowing the adherent cells to migrate from the bare vertical plane to the coated one. The cells were continuously incubated for 1 day in complete medium with or without of NO donor. Finally, the migrated cells were stained with rhodamine and observed using a fluorescence microscope.

4.5 Hemocompatibility evaluation by ex vivo blood circulation.

The *ex vivo* blood circulation was performed as described before [28]. All operation procedures of animal experiments were performed in compliance with the Chinese Council on Guide for the Care and Use of Laboratory Animals. A total of eight adult New Zealand white rabbits (2.5~3.5 kg) were used in the experiment. First, the bare and VEGF/Cu^{II}-DA-coated 316L SS foils (0.8 mm × 1 mm) were rolled up and affixed tightly onto the inner wall of a commercial PVC blood transfusion tube, which have been pre-immersed in 500U/mL heparin solution for 12 h. After general anesthesia and shaving, the left carotid artery and right jugular vein of the rabbit were exposed and then connected to the PVC tubes with samples to build an arteriovenous circuit. Each circuit contained a bifurcation, one branch was installed with a bare 316L SS foil and another with a VEGF/Cu^{II}-DA-coated foil. After 90 min circulation, all the arteriovenous circuits of the rabbits were stopped. Samples in 4 circuits were washed with PBS and fixed in 2.5% glutaraldehyde solution for SEM inspection. The other 4 circuits were rinsed with PBS. Cross-section of the tubes was photographed to calculate the occlusion rate. The thrombus was collected, photographed, and weighted.

4.6 Mechanical stability of VEGF/Cu^{II}-DA coatings and in vivo stent implantation.

Before implantation, 316L SS vascular stents coated with VEGF/Cu^{II}-DA were compressed and expanded. SEM images of the VEGF/Cu^{II}-DA coatings in different magnifications before and after compression and expansion of the vascular stent were taken to investigate their mechanical stability.

All the *in vivo* implantations of vascular stents were performed in compliance with the Chinese Council on Guide for the Care and Use of Laboratory Animals. Nine adult New Zealand white rabbits (2.5~3.5 kg) were anesthetized by 1% pentobarbital sodium. After shaving, the bilateral iliofemoral arteries of the rabbits were isolated. Bare 316L SS stents and VEGF/Cu^{II}-DA-coated stents were compressed and symmetrically implanted in the left and right iliac arteries, respectively. After implantation for 1 week, 1 and 3 months, each three stents were harvested. The stent samples harvested after 1 week were fixed in 4% paraformaldehyde, blocked with bovine serum albumin, stained with CD31/PECAM-1 antibody (Novus, NBP2-44342), phalloidin (Sigma, P1951) and DAPI (Sigma, D9542), finally scanned using laser confocal scanning microscope (Nikon, $A1R^{+}$). The relative fluorescence intensity of CD31 was calculated using

Image J. For the stent samples harvested after 1 and 3 months, each stent was transversely divided into two equal parts, one for SEM detection and the other for histomorphometric analysis. For SEM detection, the stent samples were fixed in 2.5% glutaraldehyde solution and longitudinally divided, then went through a series of processes such as dehydration, critical point drying, gold spraying and observation. For histomorphometric analysis, the stent samples were dehydrated, embedded in methacrylate solution (consisting of n-Butyl and methyl methacrylate with benzoyl peroxide), solidified and cut into 10 μm slices, and then stained with Van Gieson's solution (acid fuchsin & picric acid).

4.7 Statistical analysis.

All blood, cell, and animal assays were performed with no less than three parallel specimens. The data were presented as mean ± SD value. Statistical analysis was carried out by one-way ANOVA, with $*p < 0.05$ indicating significant statistical difference.

Author contributions

X.Z. and Z.L.Y. designed and supervised the whole project. Q.F.T, X.Z., Q.Z., S.L., X.Y.L., and K.Q.X. performed the research and experiments. X.Z., Q.Z., Q.F.T., N.H., and Z.L.Y. analyzed the data and wrote the manuscript. All the authors revised the manuscript and approved the submission.

Notes

The authors declare no competing financial interest.

Acknowledgments

This work was supported by the National Natural Science Foundation of China (31570957); International Cooperation Project by Science and Technology Department of Sichuan Province (2019YFH0103); and start-up fund (1-ZE7S) and central research fund (G-YBWS) from the Hong Kong Polytechnic University. We would like to thank Analytical and Testing Center of Southwest Jiaotong University for scanning electron microscope and laser confocal microscope detection.

Appendix A. Supplementary data

Supplementary material related to this article can be found, in the online version, at doi: XXX

Data availability

Data not available. Data will be made available on request.

Rreferences

[1] P. Joseph, D. Leong, M. Mckee, S.S. Anand, J.D. Schwalm, K. Teo, A. Mente, S. Yusuf, Reducing the global burden of cardiovascular disease, Part 1: the epidemiology and risk factors, Circ. Res. 121 (2017) 677-694.
[2] T.R. Frieden, M.G. Jaffe, Saving 100 million lives by improving global treatment of hypertension and reducing cardiovascular disease risk factors, J. Clin. Hypertens. 20 (2018) 208-211.
[3] F. Otsuka, A.V. Finn, S.K. Yazdani, M. Nakano, F.D. Kolodgie, R. Virmani, The importance of the endothelium in atherothrombosis and coronary stenting, Nat. Rev. Cardiol. 9 (2012) 439-453.
[4] T. Palmerini, U. Benedetto, G. Biondi-Zoccai, D. Della Riva, L. Bacchi-Reggiani, P.C. Smits, G.J. Vlachojannis, L.O. Jensen, E.H. Christiansen, K. Berencsi, Long-term safety of drug-eluting and bare-metal stents: evidence from a comprehensive network meta-analysis, J. Am. Coll. Cardiol. 65 (2015) 2496-2507.
[5] V. Farooq, B.D. Gogas, P.W. Serruys, Restenosis: delineating the numerous causes of drug-eluting stent restenosis, Circ. Cardiovasc Interv. 4 (2011) 195-205.
[6] M. Joner, A.V. Finn, A. Farb, E.K. Mont, F.D. Kolodgie, E. Ladich, R. Kutys, K. Skorija, H.K. Gold, R. Virmani, Pathology of drug-eluting stents in humans: delayed healing and late thrombotic risk, J. Am. Coll. Cardiol. 48 (2006) 193-202.
[7] G. Nakazawa, A.V. Finn, M. Joner, E. Ladich, R. Kutys, E.K. Mont, H.K. Gold, A.P. Burke, F.D. Kolodgie, R. Virmani, Delayed arterial healing and increased late stent thrombosis at culprit sites after drug-eluting stent placement for acute myocardial infarction patients: an autopsy study, Circulation 118 (2008) 1138-1145.
[8] K.H. Mak, G. Belli, S.G. Ellis, D.J. Moliterno, Subacute stent thrombosis: evolving issues and current concepts, J. Am. Coll. Cardiol. 27 (1996) 494-503.
[9] C. Chaabane, F. Otsuka, R. Virmani, M.L. Bochaton-Piallat, Biological responses in stented arteries, Cardiovasc. Res. 99 (2013) 353-363.
[10] F.G. Welt, C. Rogers, Inflammation and restenosis in the stent era, Arterioscler. Thromb. Vasc. Biol. 22 (2002) 1769-1776.
[11] C.C. Mohan, A.M. Cherian, S. Kurup, J. Joseph, M.B. Nair, M. Vijayakumar, S.V. Nair, D. Menon, Stable titania nanostructures on stainless steel coronary stent surface for enhanced corrosion resistance and endothelialization, Adv. Healthc. Mater. 6 (2017) 1601353.
[12] C. Liang, Y. Hu, H. Wang, D. Xia, Q. Li, J. Zhang, J. Yang, B. Li, H. Li, D. Han, Biomimetic cardiovascular stents for in vivo re-endothelialization, Biomaterials 103

(2016) 170-182.
[13] A. Habib, A.V. Finn, Endothelialization of drug eluting stents and its impact on dual anti-platelet therapy duration, Pharmacol. Res. 93 (2015) 22-27.
[14] H. Bai, J. Masuda, Y. Sawa, S. Nakano, R. Shirakura, Y. Shimazaki, J. Ogata, H. Matsuda, Neointima formation after vascular stent implantation. Spatial and chronological distribution of smooth muscle cell proliferation and phenotypic modulation, Arterioscler. Thromb. 14 (1994) 1846-1853.
[15] D.E. Drachman, E.R. Edelman, P. Seifert, A.R. Groothuis, D.A. Bornstein, K.R. Kamath, M. Palasis, D. Yang, S.H. Nott, C. Rogers, Neointimal thickening after stent delivery of paclitaxel: change in composition and arrest of growth over six months, J. Am. Coll. Cardiol. 36 (2000) 2325-2332.
[16] M.S. Kim, L.S. Dean, In-stent restenosis, Cardiovasc. Ther. 29 (2011) 190-198.
[17] K. Zhang, T. Liu, J.A. Li, J.Y. Chen, J. Wang, N. Huang, Surface modification of implanted cardiovascular metal stents: from antithrombosis and antirestenosis to endothelialization, J. Biomed. Mater. Res. A. 102 (2014) 588-609.
[18] Y. Wei, Y. Ji, L.L. Xiao, Q.K. Lin, J.P. Xu, K.F. Ren, J. Ji, Surface engineering of cardiovascular stent with endothelial cell selectivity for in vivo re-endothelialisation, Biomaterials 34 (2013) 2588-2599.
[19] H. Lee, S.M. Dellatore, W.M. Miller, P.B. Messersmith, Mussel-inspired surface chemistry for multifunctional coatings, Science 318 (2007) 426-430.
[20] M.A. Elnaggar, S.H. Seo, S. Gobaa, K.S. Lim, I.H. Bae, M.H. Jeong, D.K. Han, Y.K. Joung, Nitric oxide releasing coronary stent: a new approach using layer-by-layer coating and liposomal encapsulation, Small 12 (2016) 6012-6023.
[21] M.A. Elnaggar, R. Subbiah, D.K. Han, Y.K. Joung, Lipid-based carriers for controlled delivery of nitric oxide, Expet Opin. Drug Deliv. 14 (2017) 1341-1353.
[22] B. Gunasekera, C. Abou Diwan, G. Altawallbeh, H. Kalil, S. Maher, S. Xu, M. Bayachou, Functional layer-by-layer thin films of inducible nitric oxide (NO) synthase oxygenase and polyethylenimine: modulation of enzyme loading and NO-release activity, ACS Appl. Mater. Interfaces 10 (2018) 7745-7755.
[23] Z. Wang, Y. Lu, K. Qin, Y. Wu, Y. Tian, J. Wang, J. Zhang, J. Hou, Y. Cui, K. Wang, Enzyme-functionalized vascular grafts catalyze in-situ release of nitric oxide from exogenous NO prodrug, J. Control. Release 210 (2015) 179-188.
[24] F. Sharif, S.O. Hynes, K. McCullagh, S. Ganley, U. Greiser, P. McHugh, J. Crowley, F. Barry, T. O'brien, Gene-eluting stents: non-viral, liposome-based gene delivery of eNOS to the blood vessel wall in vivo results in enhanced endothelialization but does not reduce restenosis in a hypercholesterolemic model, Gene. Ther. 19 (2012) 321.
[25] C. Napoli, F. de Nigris, S. Williams-Ignarro, O. Pignalosa, V. Sica, L.J. Ignarro, Nitric oxide and atherosclerosis: an update, Nitric Oxide 15 (2006) 265-279.
[26] Z. Yang, Y. Yang, K. Xiong, X. Li, P. Qi, Q. Tu, F. Jing, Y. Weng, J. Wang, N. Huang, Nitric oxide producing coating mimicking endothelium function for multifunctional vascular stents, Biomaterials 63 (2015) 80-92.
[27] Z. Yang, Y. Yang, L. Zhang, K. Xiong, X. Li, F. Zhang, J. Wang, X. Zhao, N. Huang, Mussel-inspired catalytic selenocystamine-dopamine coatings for long-term generation of therapeutic gas on cardiovascular stents, Biomaterials 178 (2018) 1-10.

[28] F. Zhang, Q. Zhang, X. Li, N. Huang, X. Zhao, Z. Yang, Mussel-inspired dopamine-Cu^{II} coatings for sustained in situ generation of nitric oxide for prevention of stent thrombosis and restenosis, Biomaterials 194 (2019) 117-129.
[29] A.V. Finn, M. Joner, G. Nakazawa, F. Kolodgie, J. Newell, M.C. John, H.K. Gold, R. Virmani, Pathological correlates of late drug-eluting stent thrombosis, Circulation 115 (2007) 2435-2441.
[30] U. Forstermann, T. Munzel, Endothelial nitric oxide synthase in vascular disease: from marvel to menace, Circulation 113 (2006) 1708-1714.
[31] Q. Tu, X. Shen, Y. Liu, Q. Zhang, X. Zhao, M.F. Maitz, T. Liu, H. Qiu, J. Wang, N. Huang, A facile metal–phenolic–amine strategy for dual-functionalization of blood-contacting devices with antibacterial and anticoagulant properties, Mater. Chem. Front. 3 (2019) 265-275.
[32] C.K. Sen, S. Khanna, M. Venojarvi, P. Trikha, E.C. Ellison, T.K. Hunt, S. Roy, Copper-induced vascular endothelial growth factor expression and wound healing, Am. J. Physiol. Heart Circ. Physiol. 282 (2002) H1821-H1827.
[33] Y.M. Shin, Y.B. Lee, S.J. Kim, J.K. Kang, J.-C. Park, W. Jang, H. Shin, Mussel-inspired immobilization of vascular endothelial growth factor (VEGF) for enhanced endothelialization of vascular grafts, Biomacromolecules 13 (2012) 2020-2028.
[34] C.K. Poh, Z. Shi, T.Y. Lim, K.G. Neoh, W. Wang, The effect of VEGF functionalization of titanium on endothelial cells in vitro, Biomaterials 31 (2010) 1578-1585.
[35] H. Wang, Y. Wang, D. Li, Z. Liu, Z. Zhao, D. Han, Y. Yuan, J. Bi, X. Mei, VEGF inhibits the inflammation in spinal cord injury through activation of autophagy, Biochem. Biophys. Res. Commun. 464 (2015) 453-458.
[36] T. Wu, X. Chen, D. Fan, X. Pang, Development and application of metal materials in terms of vascular stents, Biomed. Mater. Eng. 25 (2015) 435-441.
[37] K. Yang, J.S. Lee, J. Kim, Y.B. Lee, H. Shin, S.H. Um, J.B. Kim, K.I. Park, H. Lee, S.W. Cho, Polydopamine-mediated surface modification of scaffold materials for human neural stem cell engineering, Biomaterials 33 (2012) 6952-6964.
[38] A. P. Dicks , D. L. Williams. Generation of nitric oxide from S-nitrosothiols using protein-bound Cu^{2+} sources. Chemistry & Biology 3 (1996) 655-659.
[39] R. Luo, Y. Liu, H. Yao, L. Jiang, J. Wang, Y. Weng, A. Zhao, N. Huang, Copper-incorporated collagen/catechol film for in situ generation of nitric oxide, ACS Biomater. Sci. Eng. 1 (2015) 771-779.
[40] H. Ceylan, A.B. Tekinay, M.O. Guler, Selective adhesion and growth of vascular endothelial cells on bioactive peptide nanofiber functionalized stainless steel surface, Biomaterials 32 (2011) 8797-8805.
[41] Z. Yang, Q. Tu, M.F. Maitz, S. Zhou, J. Wang, N. Huang, Direct thrombin inhibitor-bivalirudin functionalized plasma polymerized allylamine coating for improved biocompatibility of vascular devices, Biomaterials 33 (2012) 7959-7971.
[42] X. Li, H. Qiu, P. Gao, Y. Yang, Z. Yang, N. Huang, Synergetic coordination and catecholamine chemistry for catalytic generation of nitric oxide on vascular stents, NPG Asia Mater. 10 (2018) 482.